

South Asian summer monsoon variability during the last ~54 kyr inferred from surface water salinity and river run off proxies



D. Gebregiorgis ^{a,*}, E.C. Hathorne ^a, A.V. Sijinkumar ^b, B.Nagender Nath ^c, D. Nürnberg ^a, M. Frank ^a

^a GEOMAR Helmholtz Centre for Ocean Research Kiel, Wischhofstraße 1-3, 24148 Kiel, Germany

^b Govt. College Kasaragod, Vidyanager P.O, Kasaragod Dist., Kasaragod 671123, Kerala, India

^c CSIR-National Institute of Oceanography, Dona Paula, Goa 403004, India

ARTICLE INFO

Article history:

Received 6 October 2015

Received in revised form

30 January 2016

Accepted 10 February 2016

Available online xxx

Keywords:

South Asian monsoon

Upper ocean stratification

Mixed layer

Thermocline

ABSTRACT

The past variability of the South Asian Monsoon is mostly known from records of wind strength over the Arabian Sea while high-resolution paleorecords from regions of strong monsoon precipitation are still lacking. Here, we present records of past monsoon variability obtained from sediment core SK 168/GC-1, which was collected at the Alcock Seamount complex in the Andaman Sea. We utilize the ecological habitats of different planktic foraminiferal species to reconstruct freshwater-induced stratification based on paired Mg/Ca and $\delta^{18}\text{O}$ analyses and to estimate seawater $\delta^{18}\text{O}$ ($\delta^{18}\text{O}_{\text{sw}}$). The difference between surface and thermocline temperatures (ΔT) and $\delta^{18}\text{O}_{\text{sw}}$ ($\Delta\delta^{18}\text{O}_{\text{sw}}$) is used to investigate changes in upper ocean stratification. Additionally, Ba/Ca in *G. sacculifer* tests is used as a direct proxy for riverine runoff and sea surface salinity (SSS) changes related to monsoon precipitation on land. Our $\Delta\delta^{18}\text{O}_{\text{sw}}$ time series reveals that upper ocean salinity stratification did not change significantly throughout the last glacial suggesting little influence of NH insolation changes. The strongest increase in temperature gradients between the mixed layer and the thermocline is recorded for the mid-Holocene and indicate the presence of a significantly shallower thermocline. In line with previous work, the $\delta^{18}\text{O}_{\text{sw}}$ and Ba/Ca records demonstrate that monsoon climate during the LGM was characterized by a significantly weaker southwest monsoon circulation and strongly reduced runoff. Based on our data the South Asian Summer Monsoon (SAM) over the Irrawaddy strengthened gradually after the LGM beginning at ~18 ka. This is some 3 kyr before an increase of the Ba/Ca record from the Arabian Sea and indicates that South Asian Monsoon climate dynamics are more complex than the simple N-S displacement of the ITCZ as generally described for other regions. Minimum $\delta^{18}\text{O}_{\text{sw}}$ values recorded during the mid-Holocene are in phase with Ba/Ca marking a stronger monsoon precipitation, which is consistent with model simulations.

© 2016 Elsevier Ltd. All rights reserved.

1. Introduction

The South Asian Summer Monsoon (SAM) is a dominant feature of the global monsoon circulation that directly affects the livelihood of over a billion people residing in the region. The SAM is part of the large scale Asian monsoon system and is primarily driven by seasonal changes in land-sea thermal contrast and the annual cycle of the angle of the solar zenith (Meehl, 1994; Trenberth et al., 2000; Wang and Ding, 2008; Webster et al., 1998). The onset of the

SAM during May and June is concurrent with the reversal of meridional temperature gradients in the upper troposphere over the Tibetan Plateau and regions to the south (Li and Yanai, 1996; Meehl, 1994; Wu and Zhang, 1998; Yanai et al., 1992). This reversal is the result of differential seasonal heating of the continent and surrounding oceans, which generates a strong pressure gradient leading to large-scale shifts in the position of the Intertropical Convergence Zone (ITCZ) and the initiation of the low level cross equatorial southwest monsoon wind circulation. Consequently, a landward tropospheric cyclonic flow coupled with a persistent deep atmospheric convection causes convergence of moisture fluxes on the Indian subcontinent (Chen, 2003; Lau et al., 2000; Randel and Park, 2006), with the Bay of Bengal/Andaman Sea

* Corresponding author.

E-mail address: dyirgaw@geomar.de (D. Gebregiorgis).

and surrounding catchments being major moisture sinks (Yihui et al., 2004).

The SAM has exhibited pronounced variability over a wide range of time scales. The roles of the El Niño Southern Oscillation (ENSO) (Pant and Parthasarathy, 1981; Rasmusson and Carpenter, 1983; Webster and Yang, 1992) and Eurasian snow cover (Dickson, 1984; Hahn and Shukla, 1976; Kumar et al., 1999) on the interannual fluctuations of the SAM have been widely documented. Other studies have highlighted the combined effects of changes in the North Atlantic Oscillation (NAO) and in the Southern Oscillation (SO) on seasonal monsoon patterns (Kakade and Dugam, 2000; Viswambharan and Mohanakumar, 2014). Decadal to centennial scale variations in monsoon precipitation have been in phase with temperature fluctuations in northern high latitudes (Fleitmann et al., 2003). Monsoonal changes on millennial to longer timescales were principally driven by orbitally-induced changes in solar insolation prompting shifts in the mean position of the ITCZ (Fleitmann et al., 2007; Overpeck et al., 1996; Sirocko et al., 1993; Wang et al., 2005).

The past variability of the SAM has mostly been inferred from records of wind strength and the associated intensity of upwelling in the Arabian Sea (Caley et al., 2011; Clemens et al., 1991, 1996, 2008; Schulz et al., 1998; Ziegler et al., 2010). Several studies from the Arabian Sea have documented that the intensity of the SAM was characterised by millennial scale variations superimposed on long term glacial-interglacial variability (Overpeck et al., 1996; Schulz et al., 1998; von Rad et al., 1999). Other studies, mainly based on upwelling indices such as foraminifera (% *Globigerina bulloides*) and changes of eolian inputs, have argued that the strength and timing of the monsoon winds are primarily linked to the obliquity and precession of the Earth's orbit rather than long term glacial-interglacial variability (Clemens et al., 1991, 1996, 2010, 2008). However, interpretations relying on the wind based proxies have been challenged as monsoonal precipitation over the sub-continent depends more on the moisture content of the interhemispheric monsoon winds and their transport pathways rather than wind strength (Ruddiman, 1997; Sarkar et al., 2000). It is also clear that the application of the occurrence of microfossils as upwelling indicators is sensitive to many environmental factors, some of which are possibly unrelated to the monsoon (Clemens and Prell, 2003; Ziegler et al., 2010). As a result, considerable discrepancies with regard to the past variability of the SAM recorded by proxies from different regions remain unresolved. High-resolution proxy records from regions with strong monsoonal rainfall influence are therefore required to examine past changes of SAM intensity. In this regard, the Andaman Sea and the Bay of Bengal, where both monsoonal precipitation over the ocean and the continental runoff can be assessed, offer a unique prospect for understanding the past variability of the SAM. Despite this, relatively few studies have attempted to reconstruct SAM variability using proxy records of salinity in the Bay of Bengal (Govil and Naidu, 2011; Kudrass et al., 2001; Rashid et al., 2011) and in the Andaman Sea (Rashid et al., 2007). Kudrass et al. (2001) published a record of the SAM variability and sea surface salinity changes for the last 80 kyrs by combining $\delta^{18}\text{O}$ signatures of *Globigerinoides ruber* (*G. ruber*) and alkenone based temperature estimates. Similarly, paired $\delta^{18}\text{O}$ and Mg/Ca signals of planktonic foraminifera species were used to reconstruct seawater $\delta^{18}\text{O}$ ($\delta^{18}\text{O}_{\text{sw}}$) and to infer sea surface salinity (SSS) trends during the Last Glacial Maximum (LGM) and the deglaciation in the Bay of Bengal (Govil and Divakar Naidu, 2011; Rashid et al., 2011) and the Andaman Sea (Rashid et al., 2007). More recently, however, a growing number of studies have used Ba/Ca ratios of planktic foraminiferal tests to infer past river water discharge and estimate SSS changes (e.g. Weldeab et al., 2007, 2014). This is based on the fact that riverine runoff is enriched in

dissolved Ba relative to sea water (Bahr et al., 2013; Hall and Chan, 2004; Schmidt and Lynch-Stieglitz, 2011) and Ba incorporation into foraminiferal shells occurs in direct proportion to the corresponding seawater Ba concentration (Hönisch et al., 2011; Lea and Spero, 1992, 1994).

Here, we utilise the depth habitat preferences of different foraminifera species to investigate the freshwater-induced stratification in the Andaman Sea with paired Mg/Ca and $\delta^{18}\text{O}$ measurements on *Globigerinoides sacculifer* (*G. sacculifer*) and *Neogloboquadrina dutertrei* (*N. dutertrei*). These recorders of mixed layer and thermocline temperature ($\text{SST}_{\text{Mg/Ca}}$ and $\text{TT}_{\text{Mg/Ca}}$) and $\delta^{18}\text{O}$, respectively, are used to construct $\delta^{18}\text{O}_{\text{sw}}$ records, which approximate salinity at the respective water depth. The difference in surface and thermocline temperatures (ΔT) and $\delta^{18}\text{O}_{\text{sw}}$ ($\Delta \delta^{18}\text{O}_{\text{sw}}$) are used to infer changes in upper ocean stratification. Ba/Ca ratios of *G. sacculifer* tests are generated to assess changes in riverine runoff and provide the first such record for the Andaman Sea spanning the last ~54 kyrs.

2. Materials and methods

2.1. Oceanographic setting

The Andaman Sea is a marginal sea located in the northeastern corner of the Indian Ocean between the Malay Peninsula and the Andaman and Nicobar Islands. With a maximum water depth of 4200 m, it is connected with the Bay of Bengal and the Australasian Mediterranean Sea through several channels between the chain of the Andaman Islands and the Malacca Strait, respectively. The distribution of temperature and salinity with depth in the Andaman Sea is similar to that of the Bay of Bengal down to a depth of about 1000 m (Sarma and Narvekar, 2001). The Andaman Sea experiences strong seasonal variations in salinity due to abundant freshwater discharge from the Irrawaddy and Salween Rivers during the summer monsoon (Chapman et al., 2015). Distinct differences in deep sea temperature and salinity structure in the Andaman Sea are caused by the enclosed nature of the Andaman Basin and presence of several sills between the islands inhibiting deep water exchange between these two regions (Ramesh Babu and Sastry, 1976; Rao and Jayaraman, 1968; Sengupta et al., 1981). The Ganges–Meghna–Brahmaputra and Irrawaddy–Salween river systems on average discharge 1350 and 1000 km³ of freshwater annually to the Bay of Bengal and the Andaman Sea, respectively (Sengupta et al., 2006) thereby influencing mixed layer depth and salinity. In the Irrawaddy catchment, monsoon rains increase discharge from an average of ~12 km³/month during the winter and up to ~89 km³/month in the summer (Chapman et al., 2015). In the Andaman Sea, mean summer surface water salinity ranges between 28 and 33‰ (Zweng et al., 2013). The average near-surface temperature is 29 °C and is nearly homogenous in the mixed layer down to a depth of 50 m, below which stratification of the water masses restricts vertical mixing (Sarma and Narvekar, 2001; Uddin et al., 2014). The top of the thermocline varies seasonally between ~40 and ~60 m but is generally situated at a depth of ~50 m (Riser et al., 2008).

2.2. Core location and sample preparation

Sediment core SK 168/GC-1 (Lat. 11°42.463' N; Long. 94°29.606' E, water depth: 2064 m, core length: 4.20 m) was collected during the 168th cruise of ORV Sagar Kanya from the Alcock Seamount Complex in the Andaman Sea. A late Quaternary record of pteropod abundance and the $\delta^{18}\text{O}$ record from the surface dwelling planktic foraminiferal species *G. ruber* has previously been published (Sijinkumar et al., 2010). The age model from (Sijinkumar et al.,

2010) was constructed with 5 Accelerator Mass Spectrometer (AMS) ^{14}C dates of planktic foraminiferal tests (mixed *G. ruber* and *G. sacculifer*). The AMS ^{14}C ages were uniformly corrected for a 460 year reservoir age following Butzin et al. (2005). The age model was further refined by correlating the oxygen isotope values of *G. ruber* with the stacked reference oxygen isotope curve of Martinson et al. (1987) and constant sedimentation rates were assumed between age tie points. The average sedimentation rate for the core is 7.79 cm/kyr with variations between ~3.65 and ~10.20 cm/kyr during the MIS3/MIS2 and the Pleistocene-Holocene transitions respectively (Sijinkumar et al., 2010). This provides an average temporal resolution of ~700 yrs for the upper 2 m of the core spanning the Holocene to the MIS3/MIS2 transition. Below this section the temporal resolution is ~1.3 kyrs. The accuracy of this age model has been confirmed by comparison to the recently published benthic foraminifera $\delta^{18}\text{O}$ data for ODP 758 (Bolton et al., 2013) (Supplement Fig 1). This is also in line with a new benthic foraminifera $\delta^{18}\text{O}$ data from core SK 168/GC-1 discussed in detail in a separate publication (Sijinkumar et al., 2016). Thus, the published age model for the core is employed without any modifications.

Foraminifera samples from the core section were collected, and analyzed every 5 cm down to 2 m and every 10 cm for the remaining 2.2 m of the core. The abundance of foraminiferal specimens was limited in these clay rich sediments, particularly for *G. sacculifer*, and 15–20 specimens available per sample and 10 specimens per sample in some 4 samples were considered enough to obtain a representative geochemical signature, although ideally this would be more (Laepple and Huybers, 2013). For trace element analysis a constant and narrow size fraction of foraminifera is desired to avoid possible size dependent biases (e.g. Elderfield et al., 2002; Ni et al., 2007). Specimens of *G. sacculifer* and *N. dutertrei* were selected from the 315–400 μm size fraction and gently cracked between glass slides before being mixed and split for trace metal and stable isotopic analyses. For trace metal analysis the cracked sample was cleaned following a full reductive cleaning method (Boyle, 1981). Samples were initially repeatedly rinsed with sonication in distilled water ($18.2 \text{ m}\Omega$) and then ethanol (analytical grade) to ensure clay removal. Samples were then inspected under a binocular microscope to ensure they were free of obvious sediment contamination. Subsequently, samples were treated with ammonium citrate/hydrazine solution at 82°C for 30 mins and sample racks were placed in the ultrasonic bath for 1 min every 10 mins to maintain contact between reagents and sample. Samples were rinsed multiple times with distilled water before being transferred to new acid leached vials. Samples were then treated with oxidizing NaOH/ H_2O_2 solution at 82°C for 20 mins to remove organic matter. After three more rinses with distilled water, a weak acid leach with $100 \mu\text{L} 0.001 \text{ M HNO}_3$ was applied and followed by two rinses with distilled water. Samples were dissolved in 0.075 M nitric acid (HNO_3) ($500 \mu\text{L}$) assisted by sonication for 25 mins. Finally samples were centrifuged for 4 mins at 13,400 rpm and $400 \mu\text{L}$ of supernatant was transferred to new acid leached vials and diluted for measurement.

2.3. Foraminiferal isotopic and elemental analysis

The $\delta^{18}\text{O}$ measurements were performed using a MAT 253 mass spectrometer coupled with a Kiel IV Carbonate device (Thermo Scientific). Results were referenced to the NBS19 standard and are given on the VPDB scale. The estimated analytical error for $\delta^{18}\text{O}$ measurements was 0.05\% (1σ) based on repeated measurements of an in house standard (SHK Bremen). Seawater $\delta^{18}\text{O}$ ($\delta^{18}\text{O}_{\text{sw}}$) was calculated using the calibration equation of Bemis et al. (1998) and was corrected for global ice volume following Waelbroeck et al. (2002). $\delta^{18}\text{O}_{\text{sw}}$ values were converted to Vienna Standard Mean

Ocean Water (VSMOW) by adding 0.27\% to $\delta^{18}\text{O}_{\text{sw}}$. Uncertainties in $\delta^{18}\text{O}_{\text{sw}}$ are estimated by propagating the errors from the *G. sacculifer* and *N. dutertrei* $\delta^{18}\text{O}$ and Mg/Ca measurements (Mohtadi et al., 2014) and on average 0.3\% .

Element/Ca ratios were measured with an Agilent 7500cs ICP-MS. In a first step Ca concentrations were measured using Sc as an internal standard and these data were used to dilute the samples to 10 ppm Ca for elemental analysis. Element/Ca ratios were calculated using intensity ratios (Rosenthal et al., 1999) that were calibrated using standards produced gravimetrically from single element solutions. The average Mg/Ca of carbonate reference material ECRM 752-1 (Greaves et al., 2008) measured during the course of the study was $3.83 \pm 0.06 \text{ mmol/mol}$ ($n = 12, 1\sigma$). Uncertainties in SST reconstructions are estimated by propagating the errors introduced by Mg/Ca measurements and the Mg/Ca-Temperature calibration equation and are on average 1°C . SST_{Mg/Ca} and TT_{Mg/Ca} estimated from Mg/Ca data for *G. sacculifer* (*G. ruber*) and *N. dutertrei* are based on a species specific calibration equation obtained from North Atlantic (Anand et al., 2003). SSS was estimated from Ba/Ca ratios of *G. sacculifer* using a function based on sea water Ba (Ba_{sw}) concentrations and salinity data obtained from the Bay of Bengal (Singh et al., 2013) and a Ba/Ca_{sw}–foraminiferal calcite partition coefficient (D_{Ba}) of 0.19 (Lea and Boyle, 1991) (See supplement Fig 2).

Clay minerals are major sources of contamination for Mg/Ca analysis of foraminifera shells (Barker et al., 2003). To exclude such biases, aluminum (Al) and iron (Fe) concentrations were carefully monitored to identify the presence of clay contaminants. For the data set presented here there is no systematic relationship between Al/Ca (or Fe/Ca) and Mg/Ca ratios indicating the absence of clay contamination. However, Al/Ca values in 8 samples were higher than in all other samples and these data were excluded from further interpretation. In a similar manner, Ba/Ca values were compared with La/Ca values to check for barite contamination based on the idea that La is removed from sea water by barite formation (Garcia-Solsona et al., 2014). Ba/Ca ratios do not show a linear relationship with La/Ca ratios. However, we assume that significantly elevated Ba/Ca values ($>3 \text{ }\mu\text{mol/mol}$) in 9 samples are the result of barite contamination and were excluded from further interpretation.

3. Results

3.1. Sea surface temperatures and $\delta^{18}\text{O}$

Mg/Ca based estimates of SST (SST_{Mg/Ca}) and thermocline temperatures (TT_{Mg/Ca}) are shown in Fig. 2a. The SSTs range from $\sim 29^\circ\text{C}$ to 24°C whereas the thermocline temperatures range from 24.5°C to 19°C . Coldest SSTs are observed during MIS3 centered at 33–37 kyr and during the last glacial maximum (LGM). The average LGM SST of 25.8°C in the Andaman Sea is similar to the late Holocene (defined here as the average of the top 15 cm of the core representing the last ~2.7 kyrs) with-in the margin of error. Thermocline temperatures also do not show a distinct trend during these two time intervals. Additional *G. ruber* measurements obtained from late Holocene and LGM samples reveal similar SST trends (Fig. 2a) and indicate no significant difference between the records of the two species (paired-samples *t*-test, $p < 0.01$). Although it's difficult to distinguish such small changes from the inherent noise in the records, the deglacial warming pattern appears to have two warming steps from the onset of the last glacial termination during Heinrich Stadial 1 (HS1), (~18–15 kyrs) and to the transition from Bolling/Allerod (B/A) (~15–12.9 kyrs) and Younger Dryas (YD) (~12.9–11.7 kyrs) (Fig. 2a). The start of deglacial warming in the Andaman Sea is hard to pinpoint but peak mixed

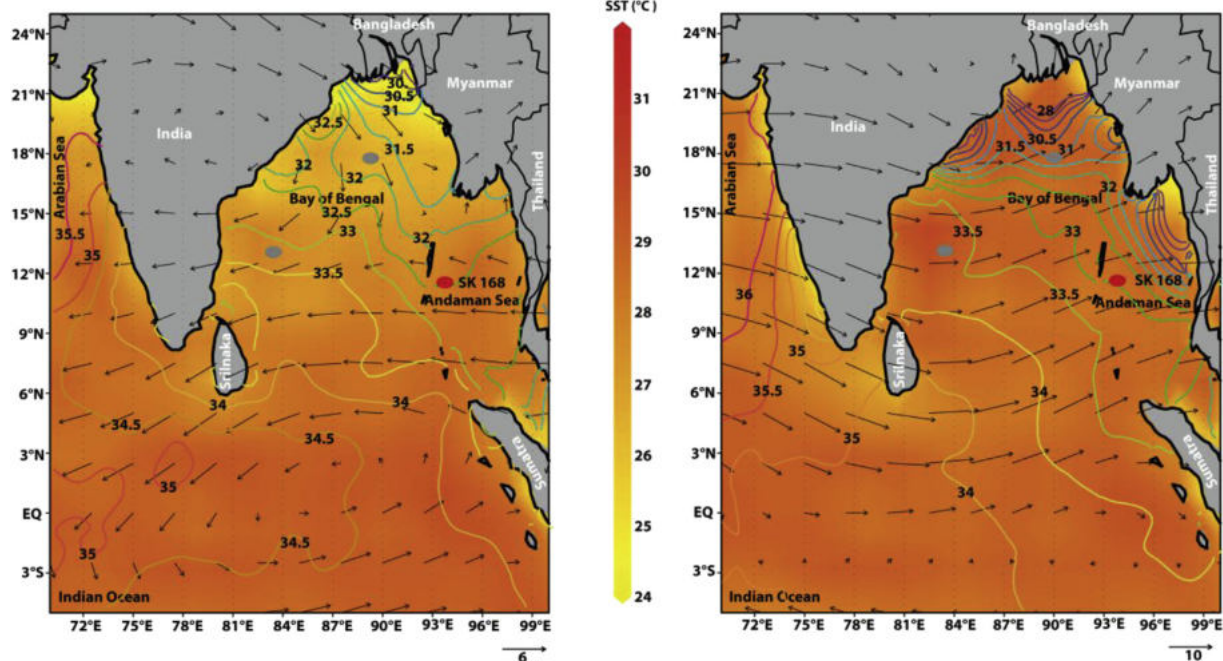


Fig. 1. Winter (left) and summer (right) sea surface temperature distribution in the Indian Ocean and eastern Arabian Sea and the location of the sediment core studied (red dot). The locations of the sediment traps studied in the Bay of Bengal (gray dots) (Gupta et al., 1997). Winter and summer SST ranges are shown in color gradient. Contour lines represent winter and summer sea surface salinities (SSS) in psu (Zweng et al., 2013). Black arrows indicate the atmospheric surface circulation pattern. Reference arrow given in m/s^{-1} . (For interpretation of the references to colour in this figure legend, the reader is referred to the web version of this article.)

layer temperatures $\sim 28^\circ C$ are reached at the onset of the B/A. SST values gradually cooled to $\sim 26^\circ C$ during the Younger Dryas (YD). After the YD values increase to a mid-Holocene maximum of $\sim 29^\circ C$ before decreasing and remaining relatively constant at $\sim 26^\circ C$ through the late Holocene.

G. sacculifer and *N. dutertrei* $\delta^{18}O$ values generally show synchronous patterns with lighter values during the mid-Holocene (~7–4 kyrs) and MIS3 (~27–54 kyrs) compared to the LGM (~23–19 kyrs) (Fig. 2b). *G. sacculifer* $\delta^{18}O$ values during MIS3 ranged from -1.7 to -0.5‰ and varied synchronously with the $\delta^{18}O$ values of *N. dutertrei*. Mean $\delta^{18}O$ values of *G. sacculifer* during the LGM progressively increased from -0.6‰ to -0.2‰ at around ~ 19 kyrs. The transition from the late glacial is marked by abrupt changes in $\delta^{18}O$ during the onset of the HS1 and the B/A. The transition from the B/A to the YD is marked by a 0.5‰ increase in $\delta^{18}O$ values centered at ~ 12 kyrs. Holocene $\delta^{18}O$ values gradually decreased and reached -2.9‰ for *G. sacculifer* and show a $\sim 2\text{‰}$ difference between the late glacial and mid-Holocene values. Late Holocene $\delta^{18}O$ values remained relatively constant and ranged between -2.5 and -2.7‰ .

3.2. Ba/Ca ratios and seawater $\delta^{18}O$

Ba/Ca and $\delta^{18}O_{SW}$ records of Core SK 168 reveal distinct changes in monsoon precipitation above the Irrawaddy catchment during the last ~ 54 kyrs (Figs. 2c and 3e). Peaks in Ba/Ca and surface *G. sacculifer* $\delta^{18}O$ ($\delta^{18}O_{SW}$) values are observed during the early part of the MIS3 and at the MIS3/2 transition centered at ~ 50 kyrs and ~ 35 kyrs, respectively. Ba/Ca gradually decreased from $\sim 1.7 \mu\text{mol/mol}$ during the MIS3/2 transition to $\sim 1 \mu\text{mol/mol}$ during the LGM which is equivalent to an SSS change from ~ 30 to 33‰ . Minimum Ba/Ca values ($0.86 \mu\text{mol/mol}$) were recorded at ~ 19 ka. The deglacial transition is marked by a relatively abrupt decrease in $\delta^{18}O_{SW}$ values during the onset of HS1 and a gradual increase in Ba/Ca and $\delta^{18}O_{SW}$ values during the B/A. Ba/Ca values gradually increased from the LGM to the mid-Holocene reaching a maximum of

$2.6 \mu\text{mol/mol}$ corresponding to a salinity minimum of $\sim 27\text{‰}$. Peak $\delta^{18}O_{SW}$ values during the mid-Holocene centered around ~ 5 kyrs were in phase with Ba/Ca peaks. Ba/Ca values during the late Holocene attained an average value of $1.7 \mu\text{mol/mol}$ corresponding to an SSS estimate of $\sim 30\text{‰}$. This is in agreement with modern summer SSS values in this region of the Andaman Sea that range between 28 and 33‰ (Zweng et al., 2013).

3.3. Vertical temperature and $\delta^{18}O_{SW}$ ($\Delta\delta^{18}O_{SW}$) gradients

Changes in vertical temperature and $\delta^{18}O_{SW}$ gradients between the *G. sacculifer* and *N. dutertrei* ($\Delta\delta^{18}O_{SW}$) are considered a measure of the density gradient between the mixed layer and thermocline and are interpreted as a proxy for upper ocean stratification. The evolution of the $\Delta\delta^{18}O_{SW}$ and the temperature gradient between the mixed layer and the thermocline are shown in Figs. 3b and c. The difference in measured $\delta^{18}O_{SW}$ between the two species ($\Delta\delta^{18}O_{SW}$) is on average 0.39‰ and ranges between -0.6 and 1.5‰ , although the uncertainties associated with these calculations are $\pm 0.5\text{‰}$. The strongest increase in $\Delta\delta^{18}O_{SW}$ values is observed during the deglacial transition centered around the B/A. The temperature gradient between the mixed layer and the thermocline ranged between ~ 1.4 and $8.3^\circ C$ with large gradients during the deglacial transition, and the mid-Holocene. The temperature gradient during the mid-Holocene was on average $\sim 7.5^\circ C$ while upper ocean density stratification remained fairly constant.

4. Discussion

4.1. Upper ocean stratification and monsoon intensity during the last glaciation

Given that the effect of global ice volume is cancelled out, the $\Delta\delta^{18}O_{SW}$ gradient between mixed layer and thermocline dwelling planktic foraminifera, a proxy for upper ocean stratification, is a

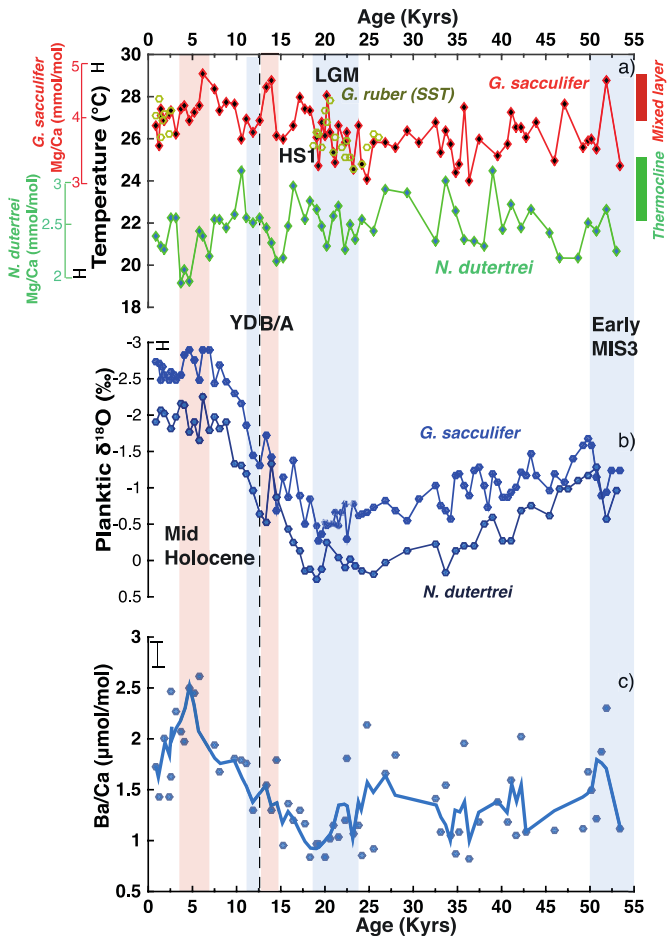


Fig. 2. a) Mg/Ca-based temperature estimates for the thermocline dwelling *N. dutertrei* (green) and the mixed layer species *G. sacculifer* (red) over the last ~54 kyrs. *G. ruber* SST_{Mg/Ca} estimates are given for LGM and late-Holocene time periods (yellow-green). The vertical bars show the range of annual SST (red) and thermocline temperatures (green) in the Andaman Sea (Locarnini et al., 2013). 1 σ -error bars are based on repeated analysis ($n = 12$) of the ECRM 752-1 standard (Greaves et al., 2008); b) Oxygen isotope ratios of foraminifera *G. sacculifer* (blue) and *N. dutertrei* (dark blue); c) Ba/Ca ratios of *G. sacculifer*. Solid line represent the 3-pts moving average. Younger Dryas (YD), Bølling–Allerød (B/A), Heinrich Stadial 1 (HS1) and last glacial maximum (LGM) are shaded based on stratigraphic boundaries defined by NGRIP (Andersen et al., 2006; Rasmussen et al., 2006). Early-MIS 3 shaded based on stratigraphic boundaries defined here (Liu et al., 2010). (For interpretation of the references to colour in this figure legend, the reader is referred to the web version of this article.)

function of local changes in $\delta^{18}\text{O}_{\text{sw}}$ of seawater. The application of the $\Delta\delta^{18}\text{O}_{\text{sw}}$ gradient to infer changes in surface water salinity stratification is dependent on the differential depth habitats of the studied foraminiferal species. Mixed layer dweller *G. sacculifer* has been observed to live and calcify with in the upper 60 m of the water column (Fairbanks et al., 1982, 1980), while *N. dutertrei* is generally most abundant in the thermocline (60–150 m) (Curry et al., 1983; Fairbanks et al., 1982). A sediment trap study conducted along a N-S transect in the Bay of Bengal (Fig. 1) suggests that the abundance of mixed layer dwelling planktic foraminifera *G. sacculifer* does not change significantly with the seasons (Gupta et al., 1997). Thermocline dwelling *N. dutertrei* is also present throughout the year and exhibits a broad peak in abundance during the initiation of the summer monsoon, directly related to the low surface salinities associated with the monsoon (Cullen, 1981; Gupta et al., 1997). Thus, seasonal biases are most likely minimal in these species and observed long-term changes in $\delta^{18}\text{O}_{\text{sw}}$ largely reflect ‘year-round’ surface and thermocline conditions. However,

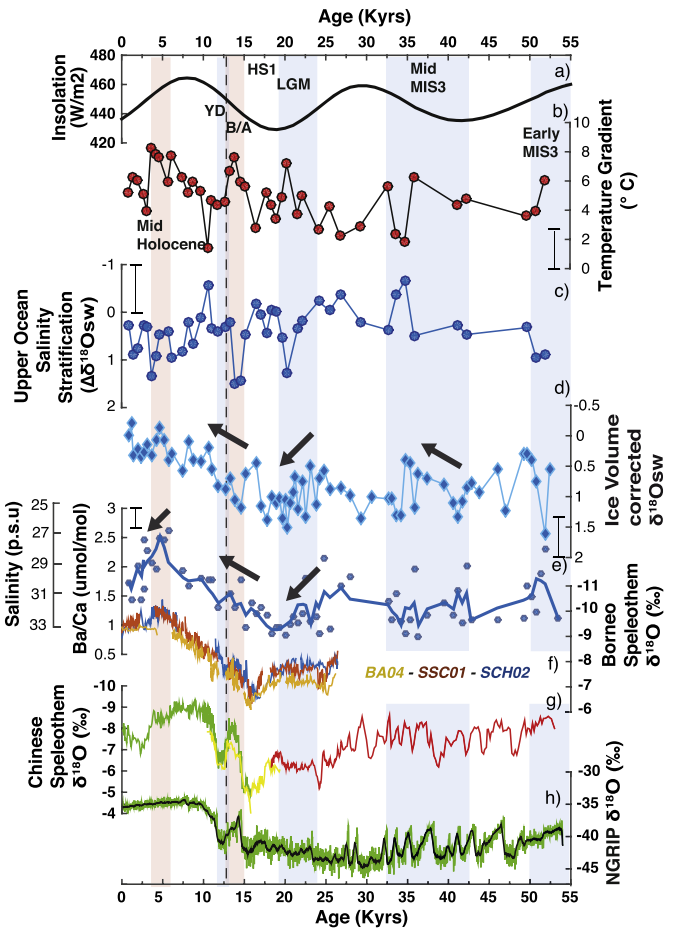


Fig. 3. SK 168 records in comparison with high resolution east Asian and south-west monsoon proxies and Greenland ice core data: a) Insolation (August) (W/m²) at 20°N (Laskar et al., 2004); b) Mixed layer and thermocline temperature gradient based on temperatures estimated using the calibration equation of Anand et al. (2003); c) $\Delta\delta^{18}\text{O}_{\text{sw}}$ record with maximum stratification plotted up; d) $\delta^{18}\text{O}_{\text{sw}}$ calculated using the calibration equation of Bemis et al. (1998) and corrected for global ice volume using (Waelbroeck et al., 2002); e) Ba/Ca ratios derived from mixed layer species *G. sacculifer* and the estimated salinity (see Supplement); f) High resolution oxygen isotopic data of stalagmites from northern Borneo (Partin et al., 2007) (g) High resolution oxygen isotopic data of stalagmites from Dongge cave (green), Hulu (PD) (yellow) and Hulu (MSD) (red) caves plotted according to their independent time scales (Wang et al., 2001; Yuan et al., 2004); h) Greenland ice core $\delta^{18}\text{O}$ chronology (NGRIP) (Svensson et al., 2008). Solid line denotes 20-pts moving average. Error bars in $\Delta\delta^{18}\text{O}_{\text{sw}}$ and ΔT estimated by propagating the error introduced by measurement uncertainties and calibration equations (Bevington and Robinson, 2003). (For interpretation of the references to colour in this figure legend, the reader is referred to the web version of this article.)

the assumption that the optimum living depth of a given species in the past has remained similar to modern day observations may not always be the case (Field, 2004; Rohling et al., 2004).

We interpret changes in the upper ocean stratification as a consequence of thermocline depth changes driven by strong wind-induced mixing and monsoon precipitation controlled upper ocean freshening, and vertical heat flux (Fig. 4). Thus, a larger/smaller ΔT gradient implies a shallower/deeper thermocline (Ravelo and Shackleton, 1995; Steinke et al., 2010; Steph et al., 2009), while $\Delta\delta^{18}\text{O}_{\text{sw}}$ minima indicates enhanced monsoon related salinity stratification. Relatively decreased temperature gradient between the mixed layer and the thermocline is recorded for the mid-MIS 3 (~35 kyrs) and indicate the presence of a deeper thermocline. However, our temperature corrected $\Delta\delta^{18}\text{O}_{\text{sw}}$ time series reveals that upper ocean salinity stratification did not change significantly when considering the uncertainties.

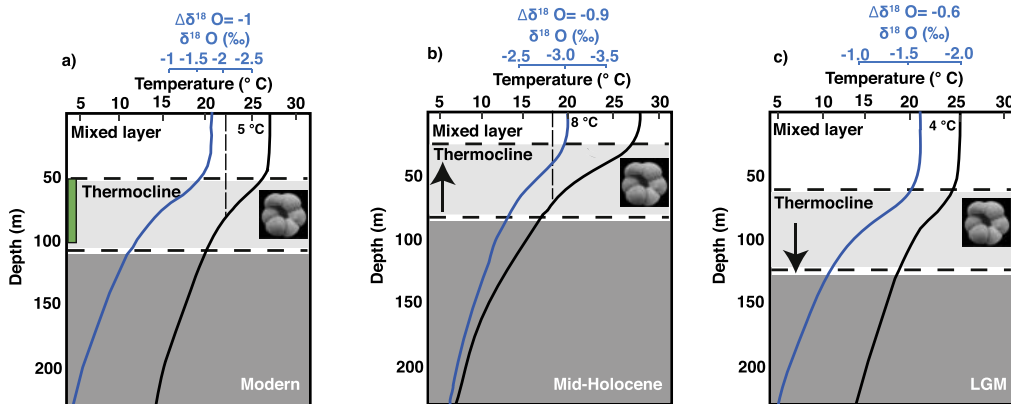


Fig. 4. Schematic illustration of changes in upper ocean stratification inferred from sea surface and thermocline temperatures and $\delta^{18}\text{O}$ values; a) Modern depth profiles of temperature and $\delta^{18}\text{O}_{\text{sw}}$ for August from World Ocean Atlas 2013 (Zweng et al., 2013). Modern $\delta^{18}\text{O}_{\text{sw}}$ values estimated from salinity and temperature data obtained from the Andaman Sea using Anand et al. (2003) and Bemis et al. (1998). Green bar shows depth range of deep chlorophyll maximum (DCM) in the northern Indian Ocean during May–June 1996 (Murty et al., 2000); Reconstructed temperature and $\delta^{18}\text{O}$ profiles for b) the mid-Holocene; c) the LGM. Mid-Holocene and LGM temperature and $\delta^{18}\text{O}_{\text{sw}}$ estimates are based on the mixed layer species *G. sacculifer* and the thermocline dwelling *N. dutertrei*. White area = mixed layer; light gray area = thermocline. (For interpretation of the references to colour in this figure legend, the reader is referred to the web version of this article.)

The climate in the SAM region has generally been described as cool and dry during the LGM (e.g. Cullen, 1981; Kudrass et al., 2001), which is supported by our higher salinity estimates for the Andaman Sea (~33‰). The physical mechanism often invoked to explain this weak SAM during the LGM is increased snow accumulation on the Tibetan Plateau causing shifts in the mean position of the ITCZ (Kudrass et al., 2001; Overpeck et al., 1996; Sirocko et al., 1996). The northeast winter monsoon circulation likely remained strong during the LGM with prevailing high-pressure cells in the Tibetan plateau (Tibet High). This is in line with lower temperatures reported for the Tibetan Plateau (Shi, 2002) and Himalaya (Mark et al., 2005) which would have weakened the meridional thermal land–sea contrast. Thus part of the weakening in SAM rainfall can be explained by an increased influence of dry continental air masses entrained by the winter monsoon. Results from phases 2 and 3 of the Paleoclimate Modeling Inter-comparison Project (PMIP2 and 3) show that SAM precipitation was reduced in all models in the LGM experiments by as much as 1.7 mm/day due to changes in NH ice sheets extent (hence a strengthened Tibetan High) and atmospheric CO₂ concentration conditions (Braconnot et al., 2007). Modern meteorological data also support this interpretation and show that an increase of snow cover on the Tibetan Plateau strengthens the high pressure cell in winter and leads to a weakened Tibetan Low and a weaker summer monsoon in the following year (Fang et al., 1999 and references therein).

4.2. The deglacial transition

The last deglaciation was punctuated by periods of Northern Hemisphere warming (B/A) and cooling (HS 1 and YD). Previous studies from the Bay of Bengal and the Arabian Sea indicate synchronous regional changes in deglacial warming and monsoon intensity remotely coupled to Greenland air temperature (Kudrass et al., 2001; Rashid et al., 2007; Schulz et al., 1998). Lighter $\delta^{18}\text{O}$ values in mixed layer dwelling planktic *G. sacculifer* marking the last deglaciation lag the changes of the surface dwelling planktic foraminifera (*G. ruber*) by ~2 kyr (Fig 5). This was also observed at ODP Site 758 in the southern Bay of Bengal (Bolton et al., 2013), and implies the slow propagation of salinity and temperature changes from surface to depth or a seasonal bias in one of the species. Deglacial Ba/Ca and $\delta^{18}\text{O}_{\text{sw}}$ trends are broadly synchronous and

indicate a gradual monsoon strengthening with the exception of the HS1. *G. sacculifer* $\delta^{18}\text{O}_{\text{sw}}$ values indicate abrupt mixed layer freshening during HS1 consistent with other studies from the Arabian Sea that reported major intensification of the southwest monsoon around 15.5 ka (e.g. Naqvi and Fairbanks, 1996; Kessarkar et al., 2010) and appears to lead abrupt upper ocean salinity stratification changes recorded for the B/A. This is in contrast to the predominantly weak east Asian monsoon inferred for the Chinese speleothem records during HS1 (e.g. Wang et al., 2001). However, the gradual SAM strengthening observed in river runoff into the Andaman Sea began ~18 kyr, leading Ba/Ca increases in the Arabian Sea around the B/A (Saraswat et al., 2013) by ~2–3 kyr (Fig 6). Together these data demonstrate SAM climate dynamics are more complex than the simple N-S displacement of the ITCZ following insolation changes as described for other regions (e.g. Overpeck et al., 1996). The SAM appears to be strongly influenced by regional scale boundary conditions altering atmospheric convection as evident from Holocene model simulations (PMIP3, Braconnot et al., 2012, Fig. 7a and b) highlighting the importance of obtaining more SST records for this region.

4.3. The Holocene

Upper ocean stratification changes during the Holocene are marked by a gradual increase in temperature gradient and shoaling of the thermocline from early to mid-Holocene in response to increased heating of the mixed layer. This is indicated by a sharp ΔT increase from ~4° to ~8 °C from the early to the mid-Holocene while $\Delta\delta^{18}\text{O}_{\text{sw}}$ gradients are marked by increased variability but did not change significantly. In contrast, $\delta^{18}\text{O}_{\text{sw}}$ values and Ba/Ca values indicate a continued strengthening of summer monsoon intensity and maximum Irrawaddy River runoff during the early to mid-Holocene. Minimum $\delta^{18}\text{O}_{\text{sw}}$ values and maximum Ba/Ca values recorded during the mid-Holocene mark the wettest period in the Andaman Sea of the past ~54 krs. A similar mid Holocene peak wetness was observed in speleothem records from northern Borneo, which has been linked to a southward shift in the mean position of the ITCZ thereby crossing the equatorial west Pacific ~5 kyr ago in response to precessional forcing (Partin et al., 2007). However, precessional forcing with a minimal lag would have resulted in the SAM maximum occurring considerably earlier between 10 and 8 kyr as seen in several palaeo precipitation records from

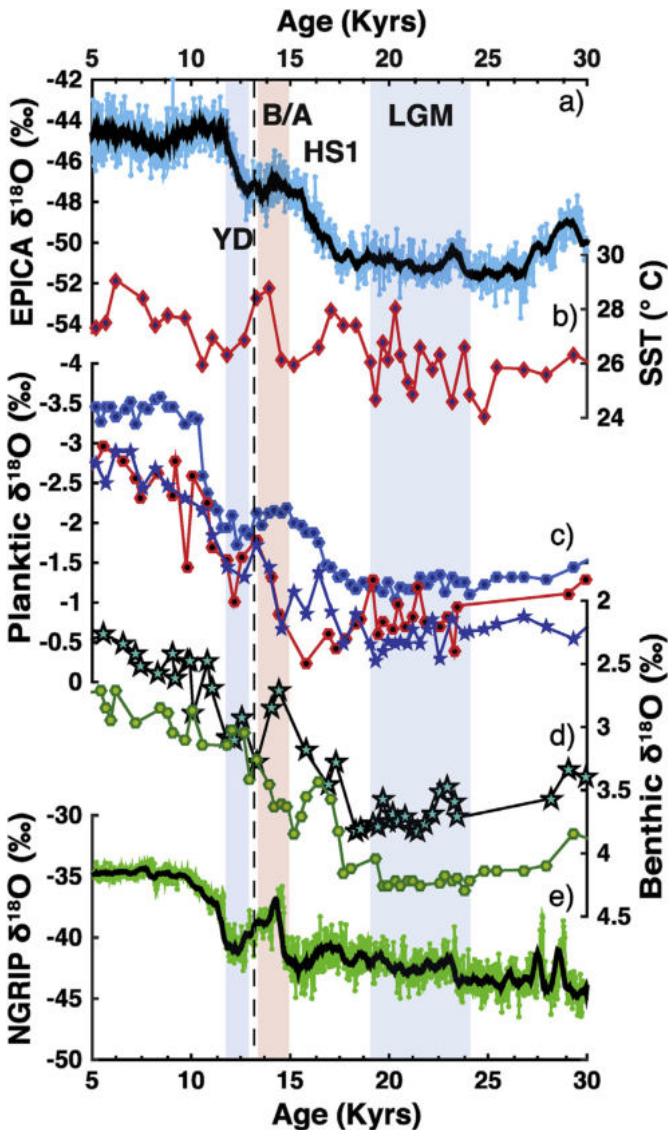


Fig. 5. Deglacial SK 168 proxy records in relation to changes in interhemispheric temperature and global ice volume. a) EPICA ice core $\delta^{18}\text{O}$ climate record (Barbante et al., 2006); b) SST_{Mg/Ca} ($^{\circ}\text{C}$) derived from *G. sacculifer*; c) $\delta^{18}\text{O}$ of *G. sacculifer* (light blue), *G. sacculifer* (stars) and NGHP 17 *G. sacculifer* records from which the Andaman Sea (red); d) Benthic (*C. wuellerstorfi*/*C. mundulus*) $\delta^{18}\text{O}$ record from NGHP 17 (star) (Ali et al., 2015) and SK 168 (green) (Sijinkumar et al., 2016, in press QSR); e) Greenland ice core $\delta^{18}\text{O}$ record (NGRIP) (Svensson et al., 2008). Solid line denotes 20-pt moving average. Shaded areas are based on stratigraphic boundaries according to (Andersen et al., 2006; Rasmussen et al., 2006). (For interpretation of the references to colour in this figure legend, the reader is referred to the web version of this article.)

north of the Equator (e.g. Stott et al., 2004; Fleitmann et al., 2003). In contrast, our records indicate that SAM precipitation peaked during the mid-Holocene thus lagging the precession minimum (at 11.5 ka) and obliquity maxima (at 9.5 kyrs) by several kyrs. Clemens et al. (1991, 1996) proposed that this large time lag between maximum NH summer insolation and the timing of strengthened SAM was governed by interhemispheric transport of latent heat from the southern subtropical Indian Ocean. Thus a combined precession and obliquity forcing of the monsoon and latent heat export associated with the two orbital bands would have strengthened SAM precipitation sometime between 9.5 and 3.5 kyrs (Clemens and Prell, 2003). This hypothesis most likely explains the mid-Holocene pacing of the monsoon observed in our

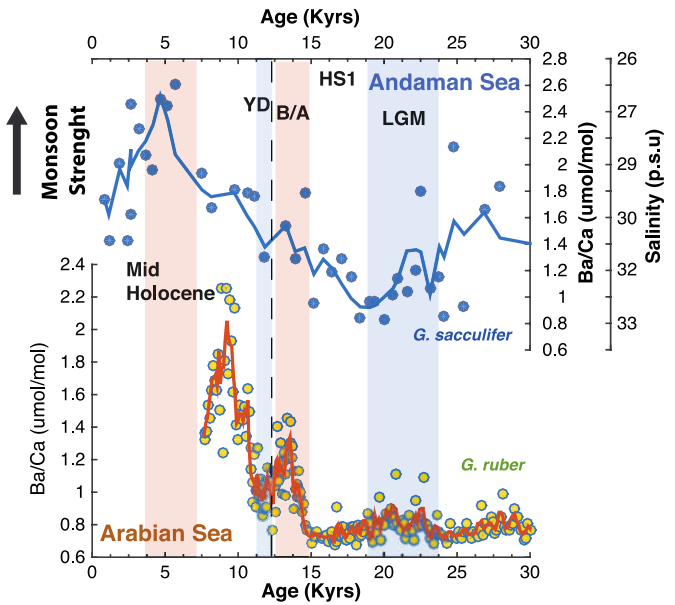


Fig. 6. SK 168 Ba/Ca record of *G. sacculifer* in comparison with high resolution Ba/Ca records of *G. ruber* from the Arabian Sea (Saraswat et al., 2013). Solid lines denotes 3-pts moving average.

records, as well as in several other high-resolution Holocene records from northwest India and Tibet (Bryson and Swain, 1981; Swain et al., 1983; Gasse et al., 1991; Gasse and Van Campo, 1994), the Arabian Sea (Fleitmann et al., 2003; Neff et al., 2001; Schulz et al., 1998), and records from other monsoon regions (Foerster et al., 2012; Weldeab et al., 2014), as well as results from the Paleoclimate Model Intercomparison Project (PMIP3, Braconnot et al., 2012). In particular, model output from the global climate model (MIROC-ESM) most competent in simulating the basic features of present day monsoon circulation (Sharmila et al., 2015) indicates mid-Holocene intensification of the SAM over the northern Indian subcontinent and Irrawaddy catchment (Fig. 7a and b). The late (4–2 ka) Holocene Ba/Ca data suggest reduction in riverine runoff while $\delta^{18}\text{O}_{\text{sw}}$ values remain stable potentially suggesting a difference in response over the oceans compared to the continent. The late Holocene weakening of the SAM possibly reflects the gradual retreat of the ITCZ in response to decreasing summer insolation (Laskar et al., 2004) as also observed in terrestrial records from India (Bryson and Swain, 1981; Swain et al., 1983; Yadava and Ramesh, 2005).

5. Conclusions

This study demonstrates that SAM climate has undergone abrupt and strong changes due to a complex interplay of orbitally induced insolation forcing and interhemispheric and regional variability. Our $\Delta\delta^{18}\text{O}_{\text{sw}}$ time series reveals that upper ocean salinity stratification did not change significantly throughout the glacial indicating a limited influence of NH insolation changes. The SAM was significantly weaker during the LGM, which is supported by heavily reduced river runoff and high SSS estimates. Deglacial Ba/Ca and $\delta^{18}\text{O}_{\text{sw}}$ trends indicate a gradual monsoon strengthening with the exception of HS1. $\delta^{18}\text{O}_{\text{sw}}$ values indicate abrupt mixed layer freshening during HS1 consistent with other studies from the Arabian Sea that reported major intensification of the southwest monsoon around 15.5 ka. However, the onset of the last deglaciation shows a gradual SAM strengthening with river runoff increasing beginning ~18 kyrs and lead observed Ba/Ca increases

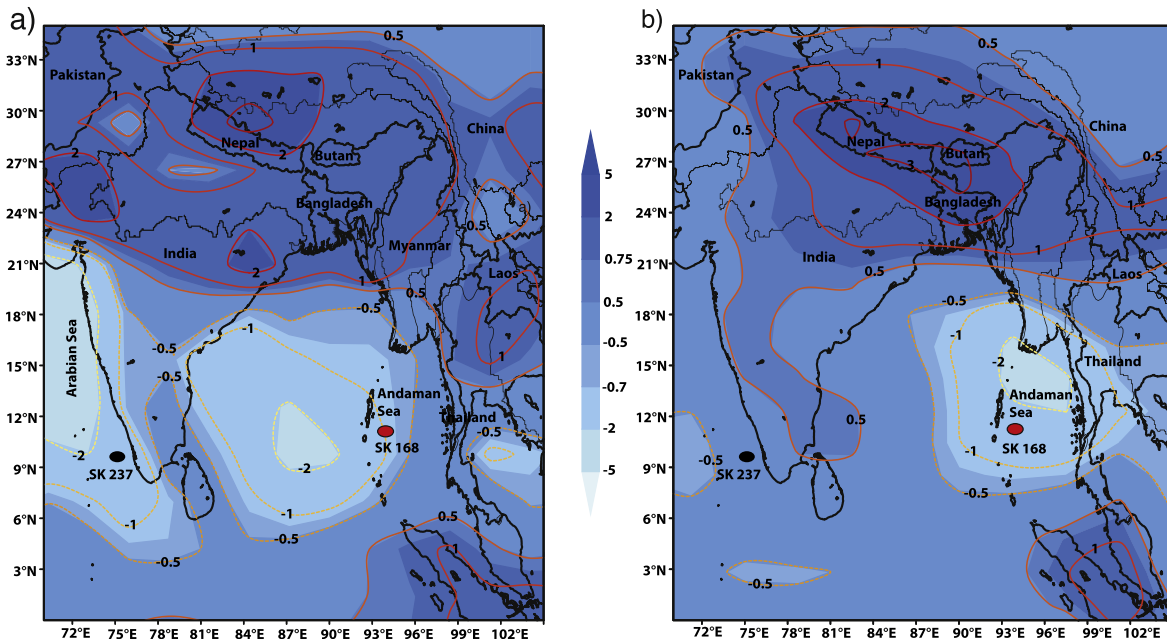


Fig. 7. Mid-Holocene JJAS mean precipitation anomalies derived from PMIP3/CMIP5 model output (color shaded) over South Asia (Braconnot et al., 2012). Dark blue (light blue) shaded areas correspond to wetter (drier) mid-Holocene conditions compared to the Pre-Industrial control run, and are expressed in millimeters per day (mm/day). a) MIROC-ESM; b) Ensemble mean. Also shown are the location of the sediment core studied (red) and core SK 237 from the Arabian sea (Saraswat et al., 2013). (For interpretation of the references to colour in this figure legend, the reader is referred to the web version of this article.)

the Arabian Sea by ~2–3 kyr. This indicates South Asian Monsoon climate dynamics are more complex than the simple N-S displacement of the ITCZ following insolation changes. Early to mid-Holocene SAM variability is characterized by a gradual intensification of monsoon rainfall while upper ocean stratification remained relatively constant. Peak monsoon strength during the mid-Holocene in the Andaman Sea is in agreement with records obtained from other monsoon regions and was most likely linked to combined precession and obliquity forcing, which is consistent with model simulations.

Acknowledgments

Part of this work was funded by the German Science Foundation, DFG, grant HA 5751/3-1. B.N. Nath thanks the Director, CSIR-National Institute of Oceanography, Goa, for the permission to publish this paper and Ministry of Earth Sciences (Government of India) for the ship time. Support from CSIR Networked Projects GEOSINKS and GENIAS is acknowledged. This is NIO contribution No. 5861. We thank Nadine Gehre for laboratory assistance for Mg/Ca cleaning and Fynn Wulf for stable isotopes measurements. We thank the two anonymous reviewers for their constructive comments, which helped us to improve the manuscript.

Appendix A. Supplementary data

Supplementary data related to this article can be found at <http://dx.doi.org/10.1016/j.quascirev.2016.02.012>.

References

- Ali, S., Hathorne, E.C., Frank, M., Gebregiorgis, D., Stattegger, K., Stumpf, R., Kutterolf, S., Johnson, J.E., Giosan, L., 2015. South Asian monsoon history over the past 60 kyr recorded by radiogenic isotopes and clay mineral assemblages in the Andaman Sea. *Geochim. Geophys. Geosys* 16 (2), 505–521.
- Anand, P., Elderfield, H., Conte, M.H., 2003. Calibration of Mg/Ca thermometry in planktonic foraminifera from a sediment trap time series. *Paleoceanography* 18 (2).
- Andersen, K.K., Svensson, A., Johnsen, S.J., Rasmussen, S.O., Bigler, M., Rothlisberger, R., Ruth, U., Siggaard-Andersen, M.-L., Steffensen, J.P., Dahl-Jensen, D., 2006. The Greenland ice core chronology 2005, 15–42 ka. Part 1: constructing the time scale. *Quat. Sci. Rev.* 25 (23), 3246–3257.
- Bahr, A., Schönfeld, J., Hoffmann, J., Voigt, S., Aurahs, R., Kucera, M., Flögel, S., Jentzen, A., Gerdes, A., 2013. Comparison of Ba/Ca and as freshwater proxies: a multi-species core-top study on planktonic foraminifera from the vicinity of the Orinoco River mouth. *Earth Planet. Sci. Lett.* 383 (0), 45–57.
- Barbante, C., Barnola, J.-M., Becagli, S., Beer, J., Bigler, M., Boutron, C., Blunier, T., Castellano, E., Cattani, O., Chappellaz, J., 2006. One-to-one coupling of glacial climate variability in Greenland and Antarctica. *Nature* 444 (7116), 195–198.
- Barker, S., Greaves, M., Elderfield, H., 2003. A study of cleaning procedures used for foraminiferal Mg/Ca paleothermometry. *Geochem. Geophys. Geosys.* 4 (9).
- Bemis, E., Spero, H.J., Bijma, J., Lea, D.W., 1998. Reevaluation of the oxygen isotopic composition of planktonic foraminifera: experimental results and revised paleotemperature equations. *Paleoceanography* 13 (2), 150–160.
- Bevington, P.R., Robinson, D.K., 2003. Data Reduction and Error Analysis, third ed. McGraw–Hill, New York, p. 320.
- Bolton, C.T., Chang, L., Clemens, S.C., Kodama, K., Ikebara, M., Medina-Elizalde, M., Paterson, G.A., Roberts, A.P., Rohling, E.J., Yamamoto, Y., 2013. A 500,000 year record of Indian summer monsoon dynamics recorded by eastern equatorial Indian Ocean upper water-column structure. *Quat. Sci. Rev.* 77, 167–180.
- Boyle, E.A., 1981. Cadmium, zinc, copper, and barium in foraminifera tests. *Earth Planet. Sci. Lett.* 53 (1), 11–35.
- Braconnot, P., Harrison, S.P., Kageyama, M., Bartlein, P.J., Masson-Delmotte, V., Abe-Ouchi, A., Otto-Bliesner, B., Zhao, Y., 2012. Evaluation of climate models using paleoclimatic data. *Nat. Clim. Change* 2 (6), 417–424.
- Braconnot, P., Otto-Bliesner, B., Kageyama, M., Kitoh, A., Lâïné, A., Loutre, M.-F., Martí, O., Merkl, U., Ramstein, G., Valdes, P., 2007. Results of PMIP2 Coupled Simulations of the Mid-Holocene and Last Glacial Maximum—part 1: Experiments and Large-scale Features.
- Bryson, R.A., Swain, A., 1981. Holocene variations of monsoon rainfall in Rajasthan. *Quat. Res.* 16 (2), 135–145.
- Butzin, M., Prange, M., Lohmann, G., 2005. Radiocarbon simulations for the glacial ocean: the effects of wind stress, Southern Ocean sea ice and Heinrich events. *Earth Planet. Sci. Lett.* 235 (1), 45–61.
- Caley, T., Malaizé, B., Zaragosi, S., Rossignol, L., Bourget, J., Eynaud, F., Martinez, P., Giradeau, J., Charlier, K., Ellouz-Zimmermann, N., 2011. New Arabian Sea records help decipher orbital timing of Indo-Asian monsoon. *Earth Planet. Sci. Lett.* 308 (3), 433–444.
- Chapman, H., Bickle, M., Thaw, S.H., Thiam, H.N., 2015. Chemical fluxes from time series sampling of the Irrawaddy and Salween Rivers, Myanmar. *Chem. Geol.* 401, 15–27.
- Chen, T.-C., 2003. Maintenance of summer monsoon circulations: a planetary-scale perspective. *J. Clim.* 16 (12), 2022–2037.
- Clemens, S., Prell, W., Murray, D., Shimmield, G., Weedon, G., 1991. Forcing mechanisms of the Indian ocean monsoon. *Nature* 353 (6346), 720–725.

- Clemens, S.C., Prell, W.L., Sun, Y., 2010. Orbital-scale timing and mechanisms driving Late Pleistocene Indo-Asian summer monsoons: reinterpreting cave speleothem $\delta^{18}\text{O}$. *Paleoceanography* 25 (4).
- Clemens, S.C., Murray, D.W., Prell, W.L., 1996. Nonstationary phase of the Plio-Pleistocene asian monsoon. *Science* 274 (5289), 943–948.
- Clemens, S.C., Prell, W.L., 2003. A 350,000 year summer-monsoon multi-proxy stack from the Owen Ridge, Northern Arabian Sea. *Mar. Geol.* 201 (1), 35–51.
- Clemens, S.C., Prell, W.L., Sun, Y., Liu, Z., Chen, G., 2008. Southern hemisphere forcing of Pliocene $\delta^{18}\text{O}$ and the evolution of Indo-Asian monsoons. *Paleoceanography* 23 (4).
- Cullen, J.L., 1981. Microfossil evidence for changing salinity patterns in the Bay of Bengal over the last 20,000 years. *Palaeogeogr. Palaeoclimatol. Palaeoecol.* 35, 315–356.
- Curry, W., Thunell, R., Honjo, S., 1983. Seasonal changes in the isotopic composition of planktonic foraminifera collected in Panama Basin sediment traps. *Earth Planet. Sci. Lett.* 64 (1), 33–43.
- Dickson, R.R., 1984. Eurasian snow cover versus Indian monsoon rainfall—An extension of the Hahn-Shukla results. *J. Clim. Appl. Meteorol.* 23 (1), 171–173.
- Elderfield, H., Vautravers, M., Cooper, M., 2002. The relationship between shell size and Mg/Ca, Sr/Ca, $\delta^{18}\text{O}$, and $\delta^{13}\text{C}$ of species of planktonic foraminifera. *Geochim. Geophys. Geosystems* 3 (8), 1–13.
- Fairbanks, R.G., Sverdrup, M., Free, R., Wiebe, P.H., Bé, A.W., 1982. Vertical Distribution and Isotopic Fractionation of Living Planktonic Foraminifera from the Panama Basin.
- Fairbanks, R.G., Wiebe, P.H., Bé, A.W., 1980. Vertical distribution and isotopic composition of living planktonic foraminifera in the western North Atlantic. *Science* 207 (4426), 61–63.
- Fang, X.-M., Ono, Y., Fukusawa, H., Bao-Tian, P., Li, J.-J., Dong-Hong, G., Oi, K., Tsukamoto, S., Torii, M., Mishima, T., 1999. Asian summer monsoon instability during the past 60,000 years: magnetic susceptibility and pedogenic evidence from the western Chinese Loess Plateau. *Earth Planet. Sci. Lett.* 168 (3), 219–232.
- Field, D.B., 2004. Variability in vertical distributions of planktonic foraminifera in the California Current: relationships to vertical ocean structure. *Paleoceanography* 19 (2).
- Fleitmann, D., Burns, S.J., Mangini, A., Mudelsee, M., Kramers, J., Villa, I., Neff, U., Al-Subbary, A.A., Buettner, A., Hippler, D., 2007. Holocene ITCZ and Indian monsoon dynamics recorded in stalagmites from Oman and Yemen (Socotra). *Quat. Sci. Rev.* 26 (1), 170–188.
- Fleitmann, D., Burns, S.J., Mudelsee, M., Neff, U., Kramers, J., Mangini, A., Matter, A., 2003. Holocene forcing of the Indian monsoon recorded in a stalagmite from southern Oman. *Science* 300 (5626), 1737–1739.
- Foerster, V., Junginger, A., Langkamp, O., Gebru, T., Asrat, A., Umer, M., Lamb, H.F., Wennrich, V., Rethemeyer, J., Nowaczyk, N., 2012. Climatic change recorded in the sediments of the Chew Bahir basin, southern Ethiopia, during the last 45,000 years. *Quat. Int.* 274, 25–37.
- Garcia-Solsona, E., Jeandel, C., Labatut, M., Lacan, F., Vance, D., Chavagnac, V., Pradoux, C., 2014. Rare earth elements and Nd isotopes tracing water mass mixing and particle-seawater interactions in the SE Atlantic. *Geochim. Cosmochim. Acta* 125, 351–372.
- Gasse, F., Arnold, M., Fontes, J.C., Fort, M., Gibert, E., Huc, A., Bingyan, L., Yuanfang, L., Qing, L., Melieres, F., 1991. A 13,000-year climate record from western Tibet. *Nature* 353 (6346), 742–745.
- Gasse, F., Van Campo, E., 1994. Abrupt post-glacial climate events in West Asia and North Africa monsoon domains. *Earth Planet. Sci. Lett.* 126 (4), 435–456.
- Govil, P., Divakar Naidu, P., 2011. Variations of Indian monsoon precipitation during the last 32kyr reflected in the surface hydrography of the Western Bay of Bengal. *Quat. Sci. Rev.* 30 (27), 3871–3879.
- Greaves, M., Caillon, N., Reubabier, H., Bartoli, G., Bohaty, S., Cacho, I., Clarke, L., Cooper, M., Daunt, C., Delaney, M., 2008. Interlaboratory comparison study of calibration standards for foraminiferal Mg/Ca thermometry. *Geochem. Geophys. Geosys.* 9 (8).
- Gupta, M., Curry, W., Ittekot, V., Muralinath, A., 1997. Seasonal variation in the flux of planktic Foraminifera; sediment trap results from the Bay of Bengal, northern Indian Ocean. *J. Foraminifer. Res.* 27 (1), 5–19.
- Hahn, D.G., Shukla, J., 1976. An apparent relationship between Eurasian snow cover and Indian monsoon rainfall. *J. Atmos. Sci.* 33 (12), 2461–2462.
- Hall, J.M., Chan, L.H., 2004. Ba/Ca in Neogloboquadrina pachyderma as an indicator of deglacial meltwater discharge into the western Arctic Ocean. *Paleoceanography* 19 (1). PA1017.
- Hönisch, B., Allen, K.A., Russell, A.D., Eggins, S.M., Bijma, J., Spero, H.J., Lea, D.W., Yu, J., 2011. Planktic foraminifers as recorders of seawater Ba/Ca. *Mar. Micropaleont.* 79 (1–2), 52–57.
- Kakade, S., Dugam, S., 2000. The simultaneous effect of NAO and SO on the monsoon activity over India. *Geophys. Res. Lett.* 27 (21), 3501–3504.
- Kessarkar, P.M., Purnachandra Rao, V., Naqvi, S., Chivas, A.R., Saino, T., 2010. Fluctuations in productivity and denitrification in the southeastern arabian sea during the late quaternary. *Curr. Sci.* 99 (4), 485–491.
- Kudrass, H., Hofmann, A., Doose, H., Emeis, K., Erlenkeuser, H., 2001. Modulation and amplification of climatic changes in the Northern Hemisphere by the Indian summer monsoon during the past 80 ky. *Geology* 29 (1), 63–66.
- Kumar, K.K., Rajagopalan, B., Cane, M.A., 1999. On the weakening relationship between the Indian monsoon and ENSO. *Science* 284 (5423), 2156–2159.
- Laepple, T., Huybers, P., 2013. Reconciling discrepancies between Uk37 and Mg/Ca reconstructions of Holocene marine temperature variability. *Earth Planet. Sci. Lett.* 375, 418–429.
- Laskar, J., Robutel, P., Joutel, F., Gastineau, M., Correia, A., Levrard, B., 2004. A long-term numerical solution for the insolation quantities of the Earth. *Astronomy Astrophysics* 428 (1), 261–285.
- Lau, K.M., Kim, K.M., Yang, S., 2000. Dynamical and boundary forcing Characteristics of regional components of the Asian summer monsoon. *J. Clim.* 13 (14), 2461–2482.
- Lea, D.W., Boyle, E.A., 1991. Barium in planktonic foraminifera. *Geochim. Cosmochim. Acta* 55 (11), 3321–3331.
- Lea, D.W., Spero, H.J., 1992. Experimental determination of barium uptake in shells of the planktonic foraminifera *Orbulina universa* at 22°C. *Geochim. Cosmochim. Acta* 56 (7), 2673–2680.
- Lea, D.W., Spero, H.J., 1994. Assessing the reliability of paleochemical tracers: barium uptake in the shells of planktonic foraminifera. *Paleoceanography* 9 (3), 445–452.
- Li, C., Yanai, M., 1996. The onset and interannual variability of the asian summer monsoon in relation to Land–Sea thermal contrast. *J. Clim.* 9 (2), 358–375.
- Liu, D., Wang, Y., Cheng, H., Edwards, R.L., Kong, X., Wang, X., Hardt, B., Wu, J., Chen, S., Jiang, X., 2010. Sub-millennial variability of Asian monsoon intensity during the early MIS 3 and its analogue to the ice age terminations. *Quat. Sci. Rev.* 29 (9), 1107–1115.
- Locarnini, R.A., A.V. Mishonov, J.I. Antonov, T.P. Boyer, H.E. Garcia, O.K. Baranova, M.M. Zweng, C.R. Paver, J.R. Reagan, D.R. Johnson, M. Hamilton, and D. Seidov, 2013. World Ocean Atlas 2013, Volume 1: Temperature. S. Levitus, Ed., A. Mishonov Technical Ed.; NOAA Atlas NESDIS 73, 40 pp.
- Mark, B., Harrison, S., Spessa, A., New, M., Evans, D., Helmens, K., 2005. Tropical snowline changes at the last glacial maximum: a global assessment. *Quat. Int.* 138, 168–201.
- Martinson, D.G., Pisias, N.G., Hays, J.D., Imbrie, J., Moore Jr., T.C., Shackleton, N.J., 1987. Age dating and the orbital theory of the ice ages: development of a high-resolution 0 to 300,000-year chronostratigraphy. *Quat. Res.* 27 (1), 1–29.
- Meehl, G.A., 1994. Coupled land-ocean-Atmosphere Processes and south asian monsoon variability. *Science* 266 (5183), 263–267.
- Mohtadi, M., Prange, M., Oppo, D.W., De Pol-Holz, R., Merkel, U., Zhang, X., Steinke, S., Lucke, A., 2014. North Atlantic forcing of tropical Indian Ocean climate. *Nature* 509 (7498), 76–80.
- Murty, V., Gupta, G., Sarma, V., Rao, B., Jyothi, D., Shastri, P., Supraveena, Y., 2000. Effect of vertical stability and circulation on the depth of the chlorophyll maximum in the Bay of Bengal during May–June, 1996. *Deep Sea Res. Part I Oceanogr. Res. Pap.* 47 (5), 859–873.
- Naqvi, W.A., Fairbanks, R.G., 1996. A 27,000 year record of Red Sea outflow: implication for timing of post-glacial monsoon intensification. *Geophys. Res. Lett.* 23 (12), 1501–1504.
- Neff, U., Burns, S., Mangini, A., Mudelsee, M., Fleitmann, D., Matter, A., 2001. Strong coherence between solar variability and the monsoon in Oman between 9 and 6 kyr ago. *Nature* 411 (6835), 290–293.
- Ni, Y., Foster, G.L., Bailey, T., Elliott, T., Schmidt, D.N., Pearson, P., Haley, B., Coath, C., 2007. A core top assessment of proxies for the ocean carbonate system in surface-dwelling foraminifers. *Paleoceanography* 22 (3).
- Overpeck, J., Anderson, D., Trumbore, S., Prell, W., 1996. The southwest Indian Monsoon over the last 18 000 years. *Clim. Dyn.* 12 (3), 213–225.
- Pant, G., Parthasarathy, S.B., 1981. Some aspects of an association between the Southern Oscillation and Indian summer monsoon. *Archives for meteorology, geophysics, and bioclimatology. Ser. B* 29 (3), 245–252.
- Partin, J.W., Cobb, K.M., Adkins, J.F., Clark, B., Fernandez, D.P., 2007. Millennial-scale trends in west Pacific warm pool hydrology since the Last Glacial Maximum. *Nature* 449 (7161), 452–455.
- Ramesh Babu, V., Sastry, J., 1976. Hydrography of the andaman sea during late winter. *Ind. J. Mar. Sci.* 5, 179–189.
- Randel, W.J., Park, M., 2006. Deep convective influence on the Asian summer monsoon anticyclone and associated tracer variability observed with Atmospheric Infrared Sounder (AIRS). *J. Geophys. Res. Atmos.* 111 (D12), D12314.
- Rao, L.G., Jayaraman, R., 1968. Hydrographical features of the southern and central Bay of Bengal during the transition period between winter and summer. *Bull. Natl. Inst. Sci. India* 38, 123–147.
- Rasmussen, S.O., Andersen, K.K., Svensson, A., Steffensen, J.P., Vinther, B.M., Clausen, H.B., Siggaard-Andersen, M.L., Johnsen, S.J., Larsen, L.B., Dahl-Jensen, D., 2006. A new Greenland ice core chronology for the last glacial termination. *J. Geophys. Res. Atmos.* (1984–2012) 111 (D6).
- Rashid, H., England, E., Thompson, L., Polyak, L., 2011. Late glacial to Holocene Indian summer monsoon variability based upon sediment. *Terr. Atmos. Ocean. Sci.* 22 (2), 215–228.
- Rashid, H., Flower, B., Poore, R., Quinn, T., 2007. A ~25ka Indian ocean monsoon variability record from the Andaman sea. *Quat. Sci. Rev.* 26 (19), 2586–2597.
- Rasmussen, E.M., Carpenter, T.H., 1983. The relationship between eastern equatorial Pacific sea surface temperatures and rainfall over India and Sri Lanka. *Mon. Weather Rev.* 111 (3), 517–528.
- Ravelo, A., Shackleton, N., 1995. Evolution of surface water circulation in the east equatorial Pacific over the past 2.0 Ma: isotopic measurements from ODP Site 851. In: *Proceeding of the Ocean Drilling Program, Scientific Results*, p. 50.
- Riser, S., Nyström, J., Rogers, A., 2008. Monsoon effects in the Bay of Bengal inferred from profiling float-based measurements of wind speed and rainfall. *Limnol. Oceanogr.* 53 (5part2), 2080–2093.
- Rohling, E., Sprovieri, M., Cane, T., Casford, J., Cooke, S., Bouloubassi, I., Emeis, K., Schiebel, R., Rogerson, M., Hayes, A., 2004. Reconstructing past planktic

- foraminiferal habitats using stable isotope data: a case history for Mediterranean sapropel S5. *Mar. Micropaleontol.* 50 (1), 89–123.
- Rosenthal, Y., Field, M.P., Sherrell, R.M., 1999. Precise determination of element/calcium ratios in calcareous samples using sector field inductively coupled plasma mass spectrometry. *Anal. Chem.* 71 (15), 3248–3253.
- Ruddiman, W.F., 1997. Tropical Atlantic terrigenous fluxes since 25,000 yrs BP. *Mar. Geol.* 136 (3), 189–207.
- Saraswat, R., Lea, D.W., Nigam, R., Mackensen, A., Naik, D.K., 2013. Deglaciation in the tropical Indian Ocean driven by interplay between the regional monsoon and global teleconnections. *Earth Planet. Sci. Lett.* 375, 166–175.
- Sarkar, A., Ramesh, R., Somayajulu, B., Agnihotri, R., Jull, A., Burr, G., 2000. High resolution Holocene monsoon record from the eastern Arabian Sea. *Earth Planet. Sci. Lett.* 177 (3), 209–218.
- Sarma, V.V.S.S., Narvekar, P.V., 2001. A study on inorganic carbon components in the Andaman Sea during the post monsoon season. *Oceanol. Acta* 24 (2), 125–134.
- Schmidt, M.W., Lynch-Stieglitz, J., 2011. Florida Straits deglacial temperature and salinity change: implications for tropical hydrologic cycle variability during the Younger Dryas. *Paleoceanography* 26 (4). PA4205.
- Schulz, H., von Rad, U., Erlenkeuser, H., von Rad, U., 1998. Correlation between Arabian Sea and Greenland climate oscillations of the past 110,000 years. *Nature* 393 (6680), 54–57.
- Sengupta, D., Bharath Raj, G.N., Shenoi, S.S.C., 2006. Surface freshwater from Bay of Bengal runoff and Indonesian through flow in the tropical Indian Ocean. *Geophys. Res. Lett.* 33 (22), L22609.
- Sengupta, R., Moraes, C., George, M., Kureishi, T., Noronha, R., Fondevila, S., 1981. Chemistry and hydrography of the Andaman Sea. *Indian J. Mar. Sci.* 10 (3), 228–233.
- Sharmila, S., Joseph, S., Sahai, A., Abhilash, S., Chattopadhyay, R., 2015. Future projection of Indian summer monsoon variability under climate change scenario: an assessment from CMIP5 climate models. *Glob. Planet. Change* 124, 62–78.
- Shi, Y., 2002. Characteristics of Late Quaternary monsoonal glaciation on the Tibetan plateau and in East Asia. *Quat. Int.* 97, 79–91.
- Sijinkumar, A., Nath, B.N., Gupta, M., 2010. Late quaternary record of pteropod preservation from the Andaman Sea. *Mar. Geol.* 275 (1), 221–229.
- Sijinkumar, A., Clemens, S., Nath, B.N., Prell, W., Benshila, R., Lengaigne, M., 2016. $\delta^{18}\text{O}$ and salinity variability from the Last Glacial Maximum to recent in the Bay of Bengal and Andaman Sea. *Quat. Sci. Rev* 135, 79–91.
- Singh, S.P., Singh, S.K., Bhushan, R., 2013. Internal cycling of dissolved barium in water column of the Bay of Bengal. *Mar. Chem.* 154, 12–23.
- Sirocko, F., Garbe-Schönberg, D., McIntyre, A., Molfino, B., 1996. Teleconnections between the subtropical monsoons and high-latitude climates during the last deglaciation. *Science* 272 (5261), 526–529.
- Sirocko, F., Sarnthein, M., Erlenkeuser, H., Lange, H., Arnold, M., Duplessy, J.C., 1993. Century-scale events in monsoonal climate over the past 24,000 years. *Nature* 364 (6435), 322–324.
- Steinke, S., Mohtadi, M., Groeneveld, J., Lin, L.C., Löwemark, L., Chen, M.T., Rendle-Bühring, R., 2010. Reconstructing the southern South China Sea upper water column structure since the Last Glacial maximum: Implications for the East Asian winter monsoon development. *Paleoceanography* 25 (2).
- Steph, S., Regenberg, M., Tiedemann, R., Multizzi, S., Nürnberg, D., 2009. Stable isotopes of planktonic foraminifera from tropical Atlantic/Caribbean core-tops: Implications for reconstructing upper ocean stratification. *Mar. Micropaleontol.* 71 (1), 1–19.
- Stott, L., Cannariato, K., Thunell, R., Haug, G.H., Koutavas, A., Lund, S., 2004. Decline of surface temperature and salinity in the western tropical Pacific Ocean in the Holocene epoch. *Nature* 431 (7004), 56–59.
- Svensson, A., Andersen, K.K., Bigler, M., Clausen, H.B., Dahl-Jensen, D., Davies, S., Johnsen, S.J., Muscheler, R., Parrenin, F., Rasmussen, S.O., 2008. A 60 000 year Greenland stratigraphic ice core chronology. *Clim. Past* 4 (1), 47–57.
- Swain, A.M., Kutzbach, J., Hastenrath, S., 1983. Estimates of Holocene precipitation for Rajasthan, India, based on pollen and lake-level data. *Quat. Res.* 19 (1), 1–17.
- Trenberth, K.E., Stepaniak, D.P., Caron, J.M., 2000. The global monsoon as seen through the Divergent atmospheric circulation. *J. Clim.* 13 (22), 3969–3993.
- Uddin, M.M., Chowdhury, M., Rahman, Z., Ahammed, S., Basak, S.C., 2014. Seasonal variability of mixed layer depth (MLD) in the Bay of Bengal. *Indian J. Geo-Mar. Sci.* 43 (3), 400–407.
- Viswambharan, N., Mohanakumar, K., 2014. Modulation of Indian summer monsoon through northern and southern hemispheric extra-tropical oscillations. *Clim. Dyn.* 1–14.
- von Rad, U., Schulz, H., Riech, V., den Dulk, M., Berner, U., Sirocko, F., 1999. Multiple monsoon-controlled breakdown of oxygen-minimum conditions during the past 30,000 years documented in laminated sediments off Pakistan. *Palaeogeogr. Palaeoclimatol. Palaeoecol.* 152 (1), 129–161.
- Waelbroeck, C., Labeyrie, L., Michel, E., Duplessy, J.C., McManus, J., Lambeck, K., Balbon, E., Labracherie, M., 2002. Sea-level and deep water temperature changes derived from benthic foraminifera isotopic records. *Quat. Sci. Rev.* 21 (1), 295–305.
- Wang, B., Ding, Q., 2008. Global monsoon: dominant mode of annual variation in the tropics. *Dyn. Atmos. Oceans* 44 (3–4), 165–183.
- Wang, P., Clemens, S., Beaufort, L., Braconnot, P., Ganssen, G., Jian, Z., Kershaw, P., Sarnthein, M., 2005. Evolution and variability of the Asian monsoon system: state of the art and outstanding issues. *Quat. Sci. Rev.* 24 (5), 595–629.
- Wang, Y.-J., Cheng, H., Edwards, R.L., An, Z., Wu, J., Shen, C.-C., Dorale, J.A., 2001. A high-resolution absolute-dated late Pleistocene monsoon record from Hulu Cave, China. *Science* 294 (5550), 2345–2348.
- Webster, P.J., Magana, V.O., Palmer, T., Shukla, J., Tomas, R., Yanai, M.U., Yasunari, T., 1998. Monsoons: processes, predictability, and the prospects for prediction. *J. Geophys. Res. Oceans* (1978–2012) 103 (C7), 14451–14510.
- Webster, P.J., Yang, S., 1992. Monsoon and ENSO: selectively interactive systems. *Q. J. R. Meteorol. Soc.* 118 (507), 877–926.
- Weldeab, S., Lea, D.W., Schneider, R.R., Andersen, N., 2007. 155,000 Years of west African monsoon and ocean thermal evolution. *Science* 316 (5829), 1303–1307.
- Weldeab, S., Menke, V., Schmiedl, G., 2014. The pace of East African monsoon evolution during the Holocene. *Geophys. Res. Lett.* 41 (5), 1724–1732.
- Wu, G., Zhang, Y., 1998. Tibetan plateau forcing and the timing of the monsoon onset over South Asia and the South China sea. *Mon. Weather Rev.* 126 (4), 913–927.
- Yadava, M., Ramesh, R., 2005. Monsoon reconstruction from radiocarbon dated tropical Indian speleothems. *Holocene* 15 (1), 48–59.
- Yanai, M., Li, C., Song, Z., 1992. Seasonal heating of the Tibetan Plateau and its effects on the evolution of the Asian summer monsoon. *J. Meteorol. Soc. Jpn.* 70 (1B), 319–351.
- Yihui, D., Chongyin, L., Yanju, L., 2004. Overview of the South China Sea monsoon experiment. *Adv. Atmos. Sci.* 21 (3), 343–360.
- Yuan, D., Cheng, H., Edwards, R.L., Dykoski, C.A., Kelly, M.J., Zhang, M., Qing, J., Lin, Y., Wang, Y., Wu, J., 2004. Timing, duration, and transitions of the last interglacial Asian monsoon. *Science* 304 (5670), 575–578.
- Zweng, M.M., J.R. Reagan, J.I. Antonov, R.A. Locarnini, A.V. Mishonov, T.P. Boyer, H.E. Garcia, O.K. Baranova, D.R. Johnson, D. Seidov, M.M. Biddle, 2013. World Ocean Atlas 2013, Volume 2: Salinity. S. Levitus, Ed., A. Mishonov Technical Ed.; NOAA Atlas NESDIS 74, 39 pp.
- Ziegler, M., Lourens, I.J., Tuenter, E., Hilgen, F., Reichart, G.J., Weber, N., 2010. Precession phasing offset between Indian summer monsoon and Arabian Sea productivity linked to changes in Atlantic overturning circulation. *Paleoceanography* 25 (3).